

# Numerical solutions to the Laser Rate Equations with noise: technical issues, implementation and pitfalls

**Lippi, G. L.; Mørk, Jesper; Puccioni, G. P.**

*Published in:*
Proceedings of SPIE

*Link to article, DOI:*
10.1117/12.2305948

*Publication date:*
2018

*Document Version*
Publisher's PDF, also known as Version of record

# Numerical solutions to the Laser Rate Equations with noise: technical issues, implementation and pitfalls

G. L. Lippi, J. Mørk, G. P. Puccioni

G. L. Lippi, J. Mørk, G. P. Puccioni, "Numerical solutions to the Laser Rate Equations with noise: technical issues, implementation and pitfalls ," Proc. SPIE 10672, Nanophotonics VII, 106722B (4 May 2018); doi: 10.1117/12.2305948

SPIE.

Event: SPIE Photonics Europe, 2018, Strasbourg, France

# Numerical solutions to the Laser Rate Equations with noise: technical issues, implementation and pitfalls

G.L. Lippi[a], J. Mørk[b], and G.P. Puccioni[c]

[a] Université Côte d'Azur, Institut de Physique de Nice, CNRS UMR 7010, Nice, France
[b]DTU Fotonik, Technical University of Denmark, 2800 Kgs. Lyngby, Denmark
[c]Istituto dei Sistemi Complessi, CNR, Via Madonna del Piano 10, I-50019 Firenze, Italy

## ABSTRACT

The stochastic implementation of the laser rate equations is discussed in detail, in light of its application to numerically predict the properties of nanolasers. The deterministic integration scheme is analysed and tested for appropriateness to the problem. The simplest stochastic, first-order scheme is considered and its particular properties and requirements are discussed. Tests for the correctness of the numerical integration are presented. Finally, thorough tests for the convergence of the stochastic integration are performed, showing their different aspects and possible pitfalls.

## 1. INTRODUCTION

Rate Equations (REs)[1,2] are one of the most successful models for the prediction and description of the dynamical response of Class B lasers[3] and have become a workhorse of numerical modeling in this field. Their impact is enormous since class B lasers represent most of the lasers currently developed and studied: solid state lasers, semiconductor-based devices (and a few notable gas lasers, such as $CO_2$).

Semiconductor-based lasers are of particular importance here since they are behind an enormous field for applications – be it in the form of edge-emitting or vertical-cavity configurations – as well as at the point of new developments in the realm of nanophotonics. As in all real systems, especially when modeling smaller devices, the role of noise can be paramount and needs to be properly accounted for. In a macroscopic description, well-suited for the investigation of larger devices, a Langevin-noise approach is common, with coefficients – computed on the basis of McCumber's theory[4,5] – which can be analytically obtained[5,6] to take into account the (stochastic) contribution of the spontaneous emission to the deterministic process. The Langevin theory, originally introduced to describe Brownian motion, is based on the assumption that the perturbations are strictly $\delta$-correlated $\langle f_i(t) f_j(t') \rangle = C\delta_{i,j}\delta(t-t')$ (for generic variables $f_i$'s and $f_j$'s, $C$ a known coefficient, $\delta_{i,j}$ is Kronecker's function and $\delta(t-t')$ the Dirac distribution). Additionally, the description holds when the system can be described in terms of continuous variables and the perturbation introduced on each variable by noise realization is small. This is realistically the case for lasers whenever the photon number is sufficiently large to consider the variation of its photon number by one unity to be negligibly small. In the threshold region, i.e., where the influence of noise is expected to play the most crucial role, this amounts to comparing the contribution of one photon to the average number of photons present in the field. Assuming a Poisson distribution for the photon emission (i.e., independent events) with $n$ photons, its average can be expressed in terms of the fraction of spontaneous emission coupled into the lasing mode[7] ($\beta$ factor) as $\langle n \rangle \approx \beta^{-1/2}$. Since in lasers with a sufficiently large cavity volume (measured in number of spontaneous emission modes $M$ resonant in a narrow frequency interval) $\beta^{-1} \approx M$, we can estimate that the quality of the Langevin approximation should be of the order of the square root of the number of cavity modes. For a specific example, considering a laser with $M \approx 10^6$ modes (a typical edge-emitting semiconductor laser), the contribution of one spontaneous photon will modify the total field intensity by a factor 0.1% at threshold where the average photon number is $O(\sqrt{\beta})$. When reducing the cavity size (thus the mode number) the approximation is expected to progressively lose its validity and problems may be expected.

Corresponding author: E-mail: gian-luca.lippi@inphyni.cnrs.fr

Nanophotonics VII, edited by David L. Andrews, Angus J. Bain, Jean-Michel Nunzi, Andreas Ostendorf,
Proc. of SPIE Vol. 10672, 106722B · © 2018 SPIE · CCC code: 0277-786X/18/$18 · doi: 10.1117/12.2305948

Surprisingly, however, the analytical predictions based on the REs modeling with Langevin noise appear to hold quite well even for lasers which approach the nanoscale.[8,9] The numerical implementation of the same equations, instead, reserve surprises;[9] thus it is crucial to check all the steps of the numerical approach to avoid perturbing the simulations with unwanted approximations.

For simplicity, in this paper we will consider the integration of REs[1] with parameter values corresponding to semiconductor lasers. The reason for this *simplification* is that the corrections brought by the terms specific to semiconductors[5] do not change the points we are going to make on the integration of the stochastic equations, thus there is no need to include additional complexity to the discussion.

No claim of mathematical rigour is made in this contribution which only aims at summarizing the main points to be checked and watched in the integration of the rate equations – something that is often done by laser physicist (even experimentalists). The only purpose is to highlight a few tools and checks which ensure a correct integration of the stochastic problem. At the end of this contribution, we will show that, in spite of all these precautions the results of the numerical integration of the REs can be misleading. Details will be given elsewhere.[9]

## 2. NUMERICAL INTEGRATION SCHEME: EULER METHOD

The choice of integration method is very important for the effectiveness and reliability of the result, on the one hand, but also for the simplicity in calculation (thus reducing the possibilities of errors) and for the computing time. We are going to analyse the suitability of first-order methods in the integration of the REs in view of including, afterwards, the stochastic terms. It is important to notice that the integration of stochastic equations with higher order methods – such as the Runge-Kutta – is a very hot topic, started many years ago, which new proposals for technical solutions which come along.[10,11] One has to keep in mind that multiplicative noise, such as the one which appears in the solution of the REs with Langevin terms, poses an even harder challenge with integration schemes of order higher than one.

In this section, we see how the Euler method is sufficiently accurate for the dynamical integration of the deterministic REs: this is good news since it allows laser physicists to perform stochastic computations without the need for sophisticated schemes which require specialized expertise. An additional consideration in favour of a first-order method is that higher-order methods (e.g. Runge-Kutta at different orders) are used to reduce the systematic errors introduced by first-order schemes. However, if noise is sufficiently large, the latter masks the errors, thus rendering the use of more complex integration techniques irrelevant.

We write the REs in the form:

$$\dot{n} = -\Gamma_c n + \beta\gamma N(n+1)\,, \tag{1}$$

$$\dot{N} = R - \beta\gamma N n - \gamma N\,, \tag{2}$$

where $n$ and $N$ represent the photon number and the carrier number, respectively, $\Gamma_c$ and $\gamma$ are the respective losses (photon decay rate, $\Gamma_c$, carrier relaxation rate, $\gamma$), $R$ is the pump rate and $\beta$ is the, already defined, fraction of spontaneous emission coupled into the lasing mode. The dot over the variables on the l.h.s. of the two equations represents the time derivative. The average contribution of the spontaneous emission to the lasing photon field is automatically accounted for by the second term (1) in the parenthesis of eq. (1).

Rescaling time to a dimensionless quantity $\tau = \Gamma_c t$ and introducing the ratio between the loss rates $\epsilon = \frac{\gamma}{\Gamma_c} \ll 1$, the REs can be recast in the following form

$$\frac{dn}{d\tau} = -\left(1-\beta\epsilon N\right) n + \beta\epsilon N\,, \tag{3}$$

$$\frac{dN}{d\tau} = \epsilon\left(P - (1+\beta n)N\right)\,, \tag{4}$$

where we have redefined a normalized pump $P = \frac{R}{\gamma}$. For clarity, we explicitely examine the case of the REs for semiconductor laser parameters, since they represent the least favourable choice of parameters for the integration

with a first-order method. In this case $\epsilon \approx O(10^{-2})$, while for solid-state lasers $\epsilon$ can span a wide range of values from $10^{-4}$ for a macroscopic cavity laser,[12] all the way to $10^{-7}$ for a microcavity device.[13]

Eq. (4) evolves on a long time scale since its derivative is defined in terms of a finite quantity multiplied by $\epsilon \ll 1$ (r.h.s.). This implies that the derivative is $O(\epsilon)$, thus small (at least $10^{-2}$ for semiconductor lasers) which leads to the slow evolution. Eq. (3), on the other hand, has a leading term with no prefactor and therefore a derivative $\epsilon^{-1}$ (i.e. $10^2$ times) larger than the partner equation.

We can loosely conclude that the dynamics is strongly damped along the "spatial" direction corresponding to the variable $n$ in phase space*. This "imbalance" between the time scales correponds to a strong dissipation in the photon field variable which ensures a fast relaxation onto the "slow" one-dimensional remaining direction of evolution. It is this rapid convergence towards the trajectory which allows for a sufficiently accurate reproduction of the true evolution using simply a first-order integration scheme†. A second element which permits the use of the Euler scheme is the fact that in order to correctly follow the trajectory, the time increment $t_s$ (step) with which the temporal progression is computed needs to be small compared to the fastest time scale, i.e. $t_s \ll \Gamma_c^{-1}$. This ensures that the "slow" evolution is followed with an even smaller time step since $\gamma \approx \epsilon\Gamma_c$. To fix ideas, if we assume $t_s = \frac{\Gamma_c^{-1}}{10}$ (the maximum possible value of $t_s$ to ensure a reasonably good reproduction of the trajectory‡), and $\epsilon = 10^{-2}$, then $t_s = \frac{\gamma^{-1}}{1000}$ – a very small time step, indeed on the slow variable§. The smallness of the step guarantees that the tangent is an excellent approximation to the actual "curved" trajectory and that the method can be used.

## 3. STOCHASTIC INTEGRATION: EULER-MARUYAMA METHOD

The inclusion of noise in the REs requires the adoption of an adapted method for the numerical integration. We begin by rewriting the REs with the noise coefficients:

$$\dot{n} = -\Gamma_c n + \beta\gamma N(n+1) + F_n(t)\,, \tag{5}$$

$$\dot{N} = R - \beta\gamma N n - \gamma N + F_N(t)\,, \tag{6}$$

written in standard notation[5] with the usual correlation properties for the noise terms:

$$\langle F_a(t)F_b(t')\rangle = 2F_{ab}\delta(t-t') \tag{7}$$

where the indices $a$ and $b$ refer to $n$ and $N$ interchangeably, the coefficients $F_{ab}$ will be defined later (eqs. (18,20–22)) and $\delta(t-t')$ is the Dirac's delta. Some care must be taken here in defining the noise processes and their role in the integration of the stochastic system of equations which ensues, since the above notation is at best misleading. An explicit definition of the noise terms will be given in the following

The second point is the numerical implementation of a stochastic scheme which includes the noise terms whose amplitudes are defined above. Notice that the coefficients have been defined on the basis of the averages of the photon and carrier numbers, thus they are only the amplitudes of the random process.

An analysis of the coefficients immediately shows that the amplitudes of the noise processes are defined as $\frac{Number^2}{time}$ where $Number$ signifies either the photon or the carrier number. Since the contribution of noise intervenes on the evolution (i.e., time derivative) of either Number (photon or carrier), then it follows that it is

*A formally more correct analysis would require finding the eigendirections (eigenvectors) if the phase space and identifying the fast and slow variables.[14,15] Given the already large difference between the two time constants, the approximate argument we have given here suffices for our discussion even for semiconductor lasers.

†The Euler scheme amounts to approximating the trajectory with the local tangent computed a the starting point at each step.

‡This allows to fix a maximum value for $t_s$. Smaller values can be taken, if needed, at the expense of a longer computing time to reproduce the same trajectory. It is good numerical practice to run a few tests, once the program is finalized, to compare the results obtained with different values of $t_s$ on a same trajectory and ensure that there are no spurious effects coming from the choice of time step.

§The quality of the approximation improves with the smallness of $\epsilon$: for solid-state lasers this is therefore even better!

inversely proportional to the square root of time, and not time itself! This is standard in all stochastic processes and follows from diffusion theory.[16,17]

For researchers who are not already experts in stochastic equations it is useful to perform a numerical test of a code that includes the noise contribution, as illustrated in the following subsection.

### 3.1 Simple test for correctness of the stochastic implementation

The reason for proposing this simple test (a more thorough one will be given later) is just to see whether the simplest programming steps work well. Researchers sufficiently experienced with integration programs may want to skip it, but we offer it for the sake of beginners who may want to use the precaution of checking the simplest step as a start, before launching into the integration of the stochastic REs. The latter indeed require accounting for correlated noise, thus handling a simple, uncorrelated one is a good starting point. We reduce the REs to a simple equation with diffusion and relaxation and propose its stochastic integration. An illustration of results with a simple diffusion process is given.

In order to test the correctness of the scheme, one can either integrate directly a diffusion process,[16] or transform the REs into a single stochastic Ordinary Differential Equation (ODE). We proceed along the second path, since we are interested in the physical problem.

Supposing a very slow relaxation of the energy reservoir (i.e., the carrier number), i.e., much slower than the times over which the diffusive process is going to be tested, one can find the equilibrium value of the carrier number

$$\overline{N} = \frac{R}{\gamma(1+\beta n)}\,, \tag{8}$$

where the overline indicates the steady state (equilibrium) solution. Substituting this expression into eq. (1), one gets:

$$\begin{aligned} \dot{n} &= -\Gamma_c n + \beta\gamma\frac{R}{\gamma(1+\beta n)}(n+1)\,, &(9)\\ &\approx -\Gamma_c n + \beta R(1+\beta n)(n+1)\,, &(10)\\ &= -\Gamma_c n + \beta R(n+1) - \beta^2 R n(n+1)\,. &(11)\end{aligned}$$

The equation can now be transformed into a stochastic one by adding a gaussian delta-correlated noise source $G$ and can be rewritten as a discrete sequence of steps, where the $k+1$-th depends on step $k$:

$$n_{k+1} = n_k - \Gamma n_k t_s + \beta R(n_k+1)t_s - \beta^2 R n_k(n_k+1) + G\sqrt{t_s}\,. \tag{12}$$

This equation displays a slower convergence than the deterministic counterpart due to the presence of the $\sqrt{t_s}$.

When computing diffusion processes, averages over multiple ($K \in \mathbb{N}$) trajectories must be taken. A suitable duration for each trajectory, to allow for sufficient diffusion, can be obtained by choosing $M_s = 10\Gamma_c t_s$. At this point, it is sufficient to run the successive evolutions and to trace the cumulative histograms of all the events.

Alternately, we can integrate a simpler but equivalent problem: simple diffusion. We therefore integrate the scalar equation:

$$\dot{x} = -\alpha x \tag{13}$$

with gaussian noise which transforms into the discrete scheme:

$$x_{n+1} = x_n - \alpha x_n + G\sqrt{t_s}\,, \tag{14}$$

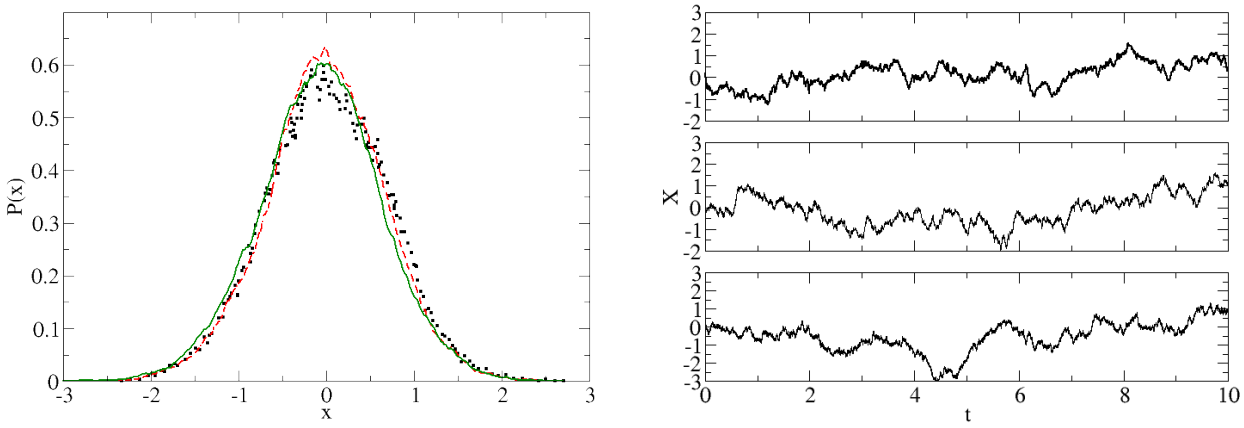


Figure 1. Left panel: histogram of the number of events obtained from a diffusion process (eqs. (13,14)) for three different time steps $t_s = 10^{-2}$ (dotted, black online), $t_s = 10^{-4}$ (dashed, red online) and $t_s = 10^{-6}$ (solid, green online) computed on a total duration $t_d = 10$ with $\alpha = 0.1$. Right panels: temporal traces computed for the same parameters and time steps, with decreasing value of the time step from top to bottom. The histogram is constructed on $N_b = 300$ bins.

where $G$ is again a delta–correlated random sequence of numbers with gaussian distribution centered around zero and unity standard deviation. Fig. 1 (left panel) shows the results of the statistical distributions for three different time steps $t_s = 10^{-2}$ (dotted, black online), $t_s = 10^{-4}$ (dashed, red online) and $t_s = 10^{-6}$ (solid, green online) computed on a total duration $t_d = 10$ with $\alpha = 0.1$. The stochastic process is correctly reproduced, as the histogram showing distribution in the values of $n$ is compatible with a gaussian (within the limits of the finite number of points). The right panel shows sample temporal traces obtained under the same conditions (cf. caption for details): the three time traces are compatible with each other, showing that the precision used in the calculation is sufficient for the reconstruction of the trajectory. Of course, it is impossible to obtain exactly the same trajectory with the three different time steps since the sequence of random numbers (even if started with the same seed) is different as it uses different numbers of calls to the random routines.

### 3.2 Implementation of the Euler-Maruyama method

Following the discussion of the preceding section, the implementation of the stochastic integration scheme, following the Euler-Maruyama method, is relatively straightforward. We proceed by rewriting the REs in vector form by defining

$$\vec{S} = \begin{pmatrix} n \\ N \end{pmatrix} \qquad \text{and} \qquad \dot{\vec{S}} = \begin{pmatrix} \dot{n} \\ \dot{N} \end{pmatrix} \tag{15}$$

thus the Stochastic REs (SREs) become

$$d\vec{S} \;\; = \;\; \mathcal{N}\vec{S}dt + \mathcal{F}d\vec{W}\,, \tag{16}$$

where $\mathcal{N}$ is the (2x2) operator which describes the deterministic dynamics of the REs, $\mathcal{F}$ the (2x2) operator describing the noise coefficients and $d\vec{W}$ is the vector of noise realizations for the two variables $n$ and $N$:

$$\mathcal{N} = \begin{pmatrix} -\Gamma_c + \beta\gamma N & \beta\gamma N \\ -\beta\gamma N & \frac{R}{N} - \gamma \end{pmatrix}, \tag{17}$$

$$\mathcal{F} = \begin{pmatrix} F_{nn} & F_{nN} \\ F_{Nn} & F_{NN} \end{pmatrix}, \tag{18}$$

$$d\vec{W} = \begin{pmatrix} G_n(0,1) \\ G_N(0,1) \end{pmatrix} d\sqrt{t_s}\,, \tag{19}$$

where $G_n(0,1)$ and $G_N(0,1)$ are two independent gaussian processes with 0 average and variance equal to 1 which represent the fluctuation in the photon variable ($G_n$) and in the carrier variable ($G_N$), respectively.

The coefficients for the noise operator $\mathcal{F}$ are the standard ones:[5]

$$F_{nn} = 2\sqrt{\beta\gamma\overline{N}(\overline{n}+1)}\,, \tag{20}$$

$$F_{nN} = F_{Nn} = -\sqrt{2\beta\gamma\overline{N}(\overline{n}+1)}\,, \tag{21}$$

$$F_{NN} = \sqrt{2(R+\gamma\overline{N}+\beta\gamma\overline{N}\overline{n})}\,, \tag{22}$$

where the bars over the variables denote the steady states, which for the REs we are handling read:

$$\overline{n} = \frac{R}{2\Gamma_c} - \frac{1}{2\beta} + \sqrt{\left(\frac{R}{2\Gamma_c} - \frac{1}{2\beta}\right)^2 + \frac{R}{\Gamma_c}}\,, \tag{23}$$

$$\overline{N} = \frac{\frac{R}{\gamma}}{1+\beta\overline{n}}\,. \tag{24}$$

These stationary solutions provide also the traditional pump value for threshold, which is obtained from eq. (23) neglecting the last term in the square root, and determining $R_{th}$ as the value for which the remaining argument of the root is zero:

$$R_{th} = \frac{\Gamma_c}{\beta}\,. \tag{25}$$

In the numerical examples that follow, we will express the pump values as a function of $R_{th}$, since this allows for comparison among different values of $\beta$

In explicit form, the Stochastic REs (SREs) become, in the Euler-Maruyama discrete implementation:

$$\begin{aligned} n_{k+1} &= n_k + (-\Gamma_c n_k + \beta\gamma N_k(n_k+1))\,t_s \\ &\quad + \left[2\sqrt{\beta\gamma\overline{N}(\overline{n}+1)}G_n^k(0,1) - \sqrt{2\beta\gamma\overline{N}(\overline{n}+1)}G_N^k(0,1)\right]\sqrt{t_s}\,, \end{aligned} \tag{26}$$

$$\begin{aligned} N_{k+1} &= N_k + (R - \beta\gamma N_k n_k - \gamma N_k)\,t_s \\ &\quad + \left[-\sqrt{2\beta\gamma\overline{N}(\overline{n}+1)}G_n^k(0,1) + \sqrt{2(R+\gamma\overline{N}+\beta\gamma\overline{N}\overline{n})}G_N^k(0,1)\right]\sqrt{t_s}\,, \end{aligned} \tag{27}$$

where $k$ represents the already computed step and $k+1$ the coming one, and where we have written out the explicit form of $\mathcal{F}d\vec{W}$ (eq. (16)). The $k$ superscript in the gaussian noise terms ($G_n^k$ and $G_N^k$) denote the $k$-th extraction for each variable. Notice that, as obvious from eqs. (16,18,19), in the computation of the next value of each variable, the noise contributions contain the cross-term multiplied by the random gaussian event of the other variable at the same time step.

The gaussian noise function will normally be obtained from a library routine, since it is important to use a high quality generator[¶] When the numerical integration is run for fixed parameter values (e.g., fixed pump) it is useful to precede the stochastic simulation by a deterministic scheme which allows for a good estimate of the average values $\overline{n}$ and $\overline{N}$, unless they have been already obtained from the steady-state expressions[‖].

This scheme is the simplest one for the stochastic implementation of a first-order (Euler) integration scheme[**]. Its performance is satisfactory whenever the stability of the numerical trajectories is good, i.e., when the equations are integrated for parameter ranges where the noise is not too large and the behaviour is regular. Its convergence may, however, be insufficient when applied in more critical situations, in particular if one is interested in specific trajectories, rather than in the average properties of independent trajectories considered as an ensemble (e.g. statistics).

One important point concerns the *reliability* of the predictions which can be obtained from the stochastic integration. Two different kinds of convergence are defined:[19]

a. *Weak convergence* means that the numerical results are significant in a statistical sense. In other words, the ensemble information is correctly reproduced, without guarantee on the details of a single trajectory.

b. *Strong convergence* means that the predictions are significant at the level of the individual trajectory, which is satisfactorily reproduced in the presence of noise.

All numerical schemes possess, *a priori*, different orders of convergence depending whether one is interested in the ensemble (*weak convergence*) or in the detailed (*strong convergence*) predictions.

For the Euler-Maruyama method, *weak convergence* is $O(1)$: decreasing the integration time steps by two orders of magnitude increases the precision in the statistical predictions by the same two orders of magnitude. As far as *strong convergence* is concerned, instead, the order is 0.5: decreasing the integration time step by a factor 100 improves the precision in the detailed predictions (trajectories) only by a factor 10.

## 4. TESTING THE STOCHASTIC CONVERGENCE

As stated above, it is of paramount importance to make sure that the convergence of the scheme is correct when integrating the stochastic REs. Independently of the previous test (Section 3.1), we need to see whether the time step selected on the basis of the considerations of Section 2 and of the implementation of the Euler-Maruyama method (Section 3.2) hold in practice. In order to do so, we run the stochastic equations (eqs. (26),27)) for a true laser. We will focus on the case of a *marginal* nanolaser (i.e., $\beta = 10^{-2}$, a "large" nanolaser) but choose a pump parameter very far from threshold to avoid all problems which may come from threshold–related effects (cf. caption of Fig. 2 for details).

A good general precaution to be used when numerically integrating differential equations is to rescale the variables and time step in such a way as to obtain numbers which are close to order 1. This avoids precision problems and round-off errors which may ensue from computations done with numbers which differ by too many orders of magnitude. For the REs and SREs we have tested both the integration with normalized variables and time step (e.g., in this case we would rescale time to the photon lifetime: $\mathcal{T} = \Gamma_c t$) and without. Programming in C language and running the programs in double precision does not show any issues related to precision or round-off, therefore we only show the results obtained with the integration of the REs in physical units. One additional piece of advice that is usually given by numerical specialists is to be careful when decreasing the integration step excessively in order to gain precision. As will become clear in the following, we have not encountered any problem even when decreasing by four orders of magnitude the time step (to gain two orders of magnitude in

[¶] In our simulations, we program the integration in C language and use GSL routines for random numbers. Cf. Section 4 for more details.

[‖] In the simple form of REs we are using here, it is preferable to use the analytical expressions for the steady states, but when simulating larger systems of equations this may become impractical and an entirely numerical approach may turn out to be simpler.

[**] Additional details on the method are available online.[18]

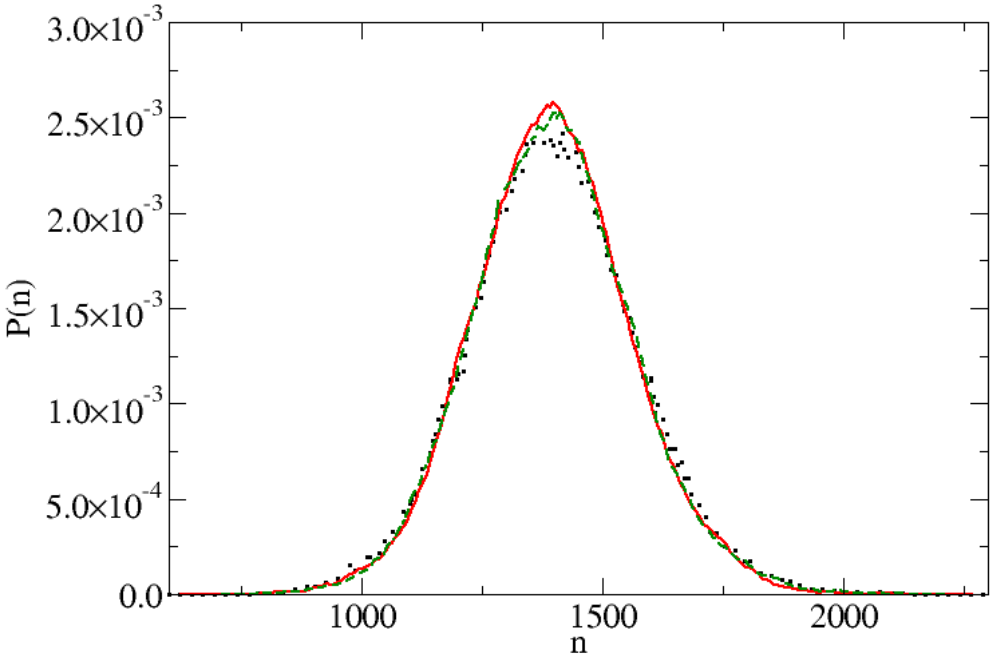


Figure 2. Histogram of the probability density of observing $n$ photons for an ensemble of 100 trajectories of duration $t_d = 1ns$ computed with time steps $t_s = 10^{-12}s$ (dots, black online), $t_s = 10^{-14}s$ (dashed, green online), and $t_s = 10^{-16}s$ (solid, red online). The histogram is constructed on $N_b = 300$ bins. Parameters: $\gamma = 1 \times 10^9 s^{-1}$, $\Gamma_c = 10^{11} s^{-1}$, $R = 15 \times R_{th}$, $\beta = 10^{-2}$.

precision on the single trajectory – cf. Section 3.2). It appears therefore that by programming in C in double precision and thanks to the nice convergence properties of the REs ("strong" intrinsic dissipation) these issues are not a serious problem with the SREs.

Noise is generated using GSL (freeware) routines with the *Mersenne Twister* algorithm:[20] the generator uses the second revision of the seeding procedure published by the authors[20] in 2002 to avoid spurious artifacts which appeared for some seed values in the original implementation. The gaussian random distribution uses the "Box-Muller" algorithm which requires two calls of the Mersenne Twister generator.

In order to test the stability of the statistical distribution with different time steps, we need to integrate the SREs with different time steps $t_s$ for a same absolute time duration $t_d$ (thus different number of points, depending on $t_s$) and accumulating over a same number $N_t$ of trajectories since each realization is issued from a random number generator initiated by one seed. This allows us to collect a statistical sample of the trajectories which explore the diffusion process induced by noise, since all other parameters are held constant during the simulation. Notice that the values of $t_s$ are chosen to match the conditions discussed in Section 2 for the largest value (indeed $t_s = \frac{\Gamma_c^{-1}}{10} = 10^{12}s$), and that the other two amount to an improvement in the strong convergence by one order of magnitude each over the previous one (cf. Section 3.2).

Furthermore, since we are eventually interested in simulating the dynamics of nanolasers, we choose a value of the $\beta$-parameter at the upper edge of the nanoscale ($\beta = 10^{-2}$) and, in order to avoid problems related to the noise size close to threshold,[9] select a pump value very far from the transition, to ensure that the Langevin approximation is well fulfilled ($R = 15 \times R_{th}$). Indeed, problems arise when integrating the SREs near threshold for meso- and nanolasers.[9]

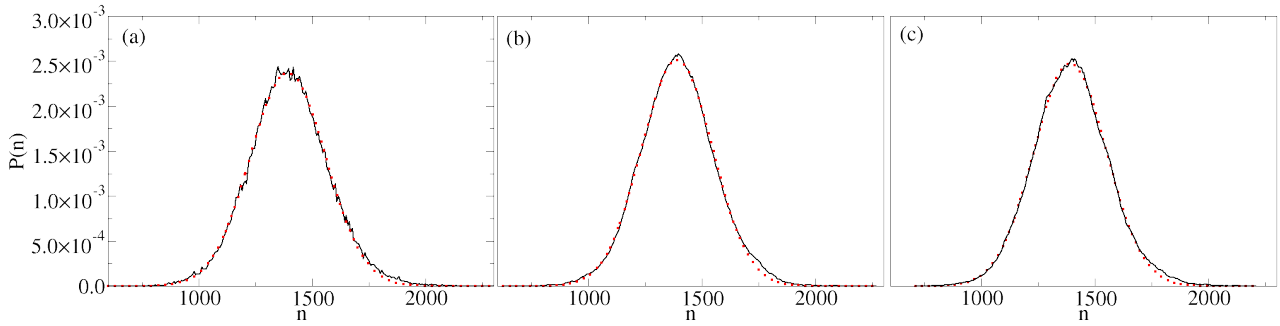


Figure 3. Stochastic distributions (solid lines, black online) as in Fig. 2, each fitted to a gaussian (dotted lines, red online). Panels: (a) $t_s = 10^{-12}s$, (b) $t_s = 10^{-14}s$, (c)$t_s = 10^{-16}s$. The vertical axis is common to all figures and is given on the left of panel (a). The results of the fit are reported on the bottom part of Table 1.

| | $t_s = 10^{-12}s$ | $t_s = 10^{-14}s$ | $t_s = 10^{-16}s$ |
|---|---|---|---|
| $\langle n \rangle$ | 1401.11 | 1399.05 | 1400.67 |
| $\sigma_n$ | 175.60 | 165.04 | 167.18 |
| $\varsigma$ | 0.087 | 0.115 | 0.117 |
| $\kappa$ | 0.223 | 0.280 | 0.296 |
| $\langle n_G \rangle$ | 1392.46 | 1392.12 | 1392.79 |
| $\sigma_{n,G}$ | 166.45 | 157.05 | 159.56 |
| $\chi^2$ | $3.4 \times 10^{-7}$ | $2.6 \times 10^{-7}$ | $2.6 \times 10^{-7}$ |
| $R$ | 0.999 | 0.999 | 0.999 |

Table 1. Summary of the features of the convergence test comparing three different integration steps of the SREs in the Euler-Maruyama scheme: $t_s = 10^{12}s$, $t_s = 10^{14}s$, and $t_s = 10^{16}s$. The data is divided into two subtables. The upper one gives indicators computed on the ensemble of data with $\langle n \rangle$ average number of photons $n$, $\sigma_n$ its standard deviations, $\varsigma$ skewness and $\kappa$ the kurtosis. The indicators in the lower subtable refer to the gaussian fits with $\langle n_G \rangle$ best fitted average, $\sigma_{n,G}$ best fit for the Gaussian's width. The parameters $\chi^2$ and $R$ represent the corresponding statistical tests.

Fig. 2 shows the histogram of the probability density of observing $n$ photons for an ensemble of $n_t = 100$ trajectories of duration $t_d = 1ns$ computed with time steps $t_s = 10^{-12}s$ (dots, black online – $10^5$ points), $t_s = 10^{-14}s$ (dashed, green online – $10^7$ points), and $t_s = 10^{-16}s$ (solid, red online – $10^9$ points). The simulations are run starting from an initial seed, which is re-initialized for each trajectory. The parameters are kept stable and the initial conditions for the deterministic variables $n$ and $N$) are their respective steady-state values for the chosen pump value. The histograms are constructed taking all the data corresponding to a different integration step and binning them (the different number of points, indicated above) results from the conditions explained above).

The statistical distributions obtained with the three integration steps are visually very similar (Fig. 2) even though the influence of the total number of points used for their construction is visible: the dotted (black online) curve is obtained from $10^5$ points only and is much noisier than the others. Visual inspection suggests, however, that the three time steps should give results which are equivalent in the statistics. Better information can be gained by fitting the three curves to a standard gaussian (expected from diffusion theory[17]) and comparing the quality of the fits. Fig. 3 shows this comparison, where the three panels correspond to the three distributions obtained with decreasing time steps from panels (a) to (c).

A quantitative analysis of the comparison is given in Table 1. The upper part of the table gives the indicators computed on the data extracted from the simulations. In addition to average photon number $\langle n \rangle$ and its standard deviation $\sigma_n$, we find the skewness $\varsigma$ and kurtosis $\kappa$ defined as:

$$\varsigma = \frac{\frac{1}{M}\sum_i (n_i - \langle n \rangle)^3}{\sigma_n^{3/2}}, \tag{28}$$

$$\kappa = \frac{\frac{1}{M}\sum_i (n_i - \langle n \rangle)^4}{\sigma_n^2}, \tag{29}$$

where $M$ is the total number of points on which the sum is carried out. The bottom half of Table 1 contains information on the fits obtained for the three distributions displayed in Fig. 3. The average and standard deviations are identified as $\langle n_G \rangle$ and $\sigma_{n,G}$, respectively (the subscript "G" referring to the Gaussian), while $\chi^2$ and $R$ are the statistical parameters which identify the goodness of the fit:

$$\chi^2 = \frac{\sum_i (n_i - n_{G,i})^2}{N_f}, \tag{30}$$

$$R^2 = 1 - \frac{\sum_i (n_i - \langle n \rangle)^2}{\sum_i (n_i - n_{G,i})^2}, \tag{31}$$

where $n_i$ represents the value in the i-th bin of the histogram and $n_{G,i}$ the corresponding value of the Gaussian distribution and $N_f$ is the number of effective degrees of freedom (approximately equivalent to the number of bins $N_b$ from which one substracts the number of parameters to be determined).

Table 1 shows that the distributions vary very little from each other, both in average $\langle n \rangle$ and standard deviation $\sigma_n$. Some residual skewness $\varsigma$ and kurtosis $\kappa$ remain in all the distributions, but the values are small. This leads to concluding that the three time steps provide equivalently good statistical coverage of the diffusive trajectories. This conclusion is further confirmed by looking at the fits (cf. Fig. 3 for visual comparison): the averages $\langle n_G \rangle$ are practically identical and within 0.6% of the corresponding numerical estimates, while the standard deviations $\sigma_{n,G}$ agree within $\approx 6\%$ both among one another and with the numerical estimates. Finally, the goodness of fit is excellent with very small, and very close, values for $\chi^2$ and nearly perfect $R^2$.

## 5. ADDITIONAL TESTS

It is useful to perform some additional tests on the performance of the integration scheme in order to have a good picture of its possible limitations. Fig. 4 shows the resulting statistics obtained from the stochastic integration of a same trajectory, i.e. run under the same conditions starting from the same initial point, but with different noise seeds. The integration time step is chosen to give a good reproduction of the statistics and the total duration of the integration is $t_d = 10ns$, thus providing $10^6$ points per histogram. The three distributions are indistinguishable thus convincingly show that the scheme works correctly.

Fig. 5 shows the statistical distribution of the photon number $n$ (solid line, black online) computed on a single trajectory with time step $t_s = 10^{-12}s$, as in Fig. 2, but on a total time $t_d = 100ns$, and compared to its gaussian fit (dashed line, red online). The numerical distribution obtained from the SREs well approaches the gaussian fit although it is noisier than the corresponding curve in Fig. 2 (in spite of the same number of points in the histograms). This is simply the result of the single trajectory computed for Fig. 5 which does not cover the phase space as densely as an ensemble of different trajectories (Fig. 2) as is well-known from diffusion theory.[17]

Temporal signals (Fig. 6) predicted by the SREs immediately show that there is a clear maximum value for the time step. In the left panel (Fig. 6) the temporal evolution of the photon number predicted with the largest time step ($t_s = 10^{-11}s$) is clearly different from the one resulting from the maximum time step ($t_s = 10^{-12}s$) allowed according to the criterion discussed in Section 2. The amplitude modulation predicted with an insufficiently small time step is largely overstimated. On the other hand, the signals predicted with time steps $t_s \leq 10^{-12}s$ give results which are compatible with one another (right panels in Fig. 6). Given the enormous number of points coming from the integration with $t_s = 10^{-16}s$ ($10^8$ to keep the duration equal to that of the other traces), it has been necessary to perform an "integration" of the information. Similarly to what is done experimentally when detecting light with a bandpass-limited detector, we have averaged the number of photons "detected" in

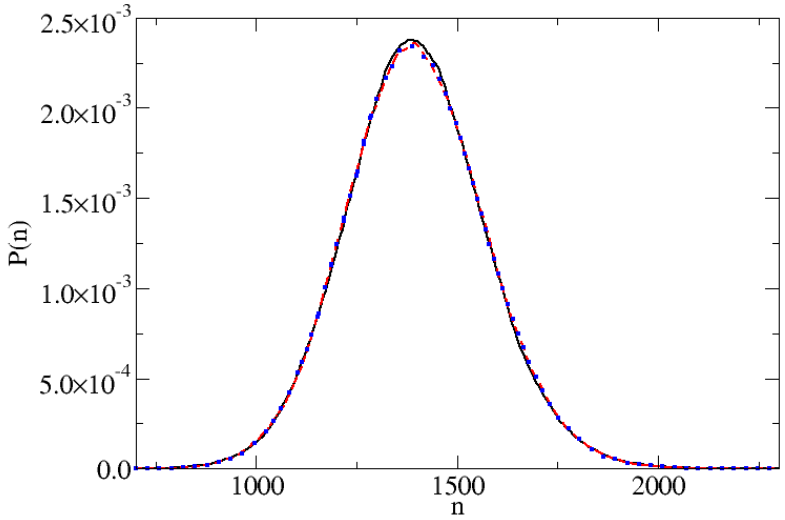


Figure 4. Histogram of the probability density of observing $n$ photons for an ensemble of 100 trajectories of duration $t_d = 10ns$ computed with time steps $t_s = 10^{-14}s$ starting from three different initial seeds for the random number generator. The histogram is constructed on $N_b = 300$ bins. Parameters: $\gamma = 1 \times 10^9 s^{-1}$, $\Gamma_c = 10^{11} s^{-1}$, $R = 15 \times R_{th}$, $\beta = 10^{-2}$.

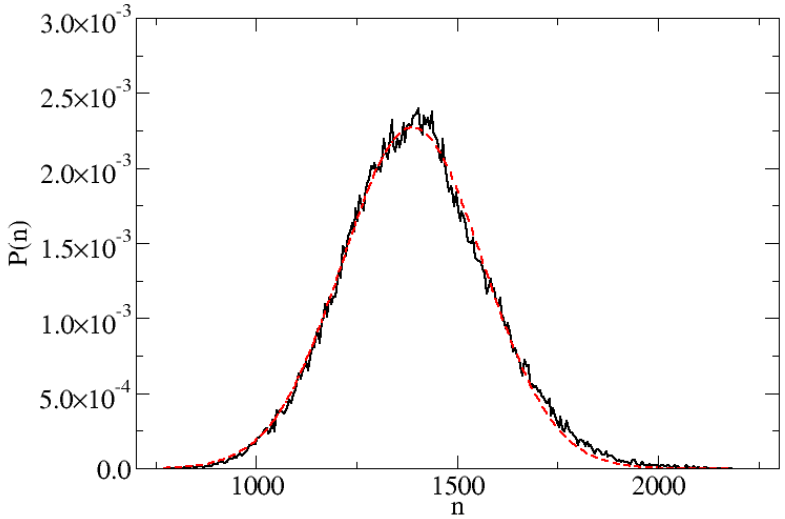


Figure 5. Histogram of the probability density of observing $n$ photons for one single trajectory of duration $t_d = 100ns$ computed with time steps $t_s = 10^{-12}s$ (solid line, black online) compared to its corresponding gaussian fit (dashed line, red online). The total number of points is the same as in Fig. 2 (dotted curve, black online) but is issued from one single trajectory. The histogram is constructed on $N_b = 300$ bins. Parameters: $\gamma = 1 \times 10^9 s^{-1}$, $\Gamma_c = 10^{11} s^{-1}$, $R = 15 \times R_{th}$, $\beta = 10^{-2}$.

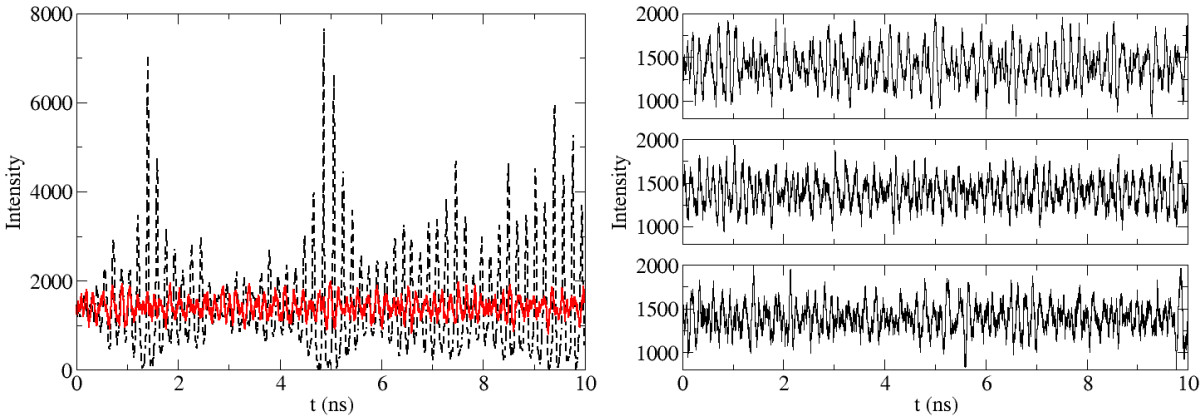


Figure 6. Temporal traces computed with the SREs using different time steps. Left panel: Right panel: $t_s = 10^{-12}s$ (top trace – same as ... in the left panel); $t_s = 10^{-14}s$ (mid trace); $t_s = 10^{-16}s$ (bottom trace) with an integration on a "detector" over a time $t_{det} = 10^{-14}s$ – cf. text for details. Parameters: $\gamma = 1 \times 10^9 s^{-1}$, $\Gamma_c = 10^{11} s^{-1}$, $R = 15 \times R_{th}$, $\beta = 10^{-2}$.

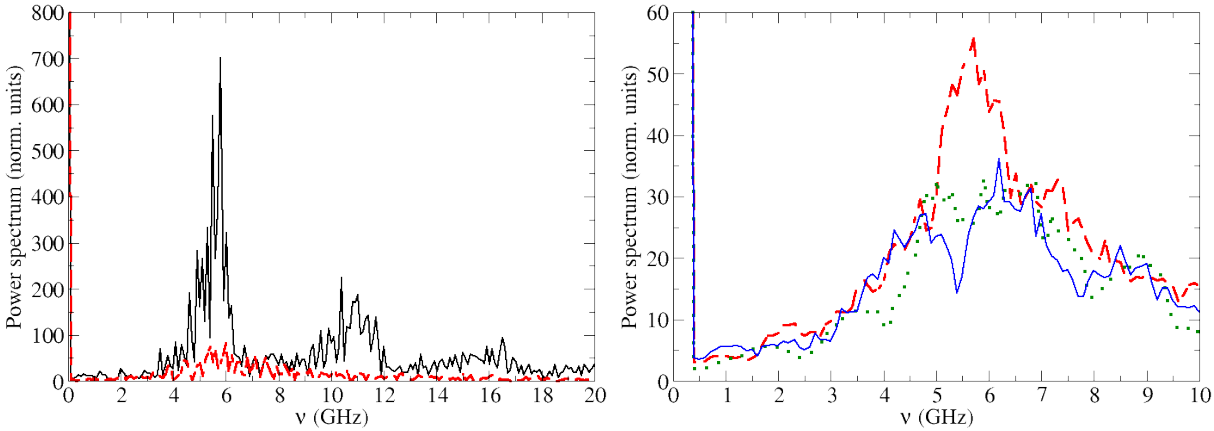


Figure 7. Power spectra of the temporal traces of Fig. 6. Left panel: integration of the SREs with $t_s = 10^{-11}s$ (solid line, black online) and with $t_s = 10^{-12}s$ (dashed line, red online). Right panel: integration of the SREs with $t_s = 10^{-12}s$ (dashed line, red online) and with $t_s = 10^{-14}s$ (dotted line, green online) and $t_s = 10^{-16}s$ (solid line, blue online). The dashed spectrum (red online) is the same in both panels for comparison. Parameters: $\gamma = 1 \times 10^9 s^{-1}$, $\Gamma_c = 10^{11} s^{-1}$, $R = 15 \times R_{th}$, $\beta = 10^{-2}$.

a time window $t_w = 10^{-14}s$, thereby obtaining a number of points equivalent to that coming from $t_s = 10^{-14}s$ (but computed with a finer time step and following the system's trajectory more accurately).

Additional information is provided by the power spectra (Fig. 7) computed on the temporal traces of Fig. 6. The left panel compares the spectrum of the signal computed with the largest time step ($t_s = 10^{-11}s$ – solid line, black online) to that of the largest step compatible with the criteria of Section 2: $t_s = 10^{-12s}$ (dashed line, red online). The two spectra are clearly incompatible, with the one obtained for the largest time step showing harmonics of a strong fundamental. This translates into spectral information what is also visible from the time trace (left panel of Fig. 6): the choice of time step *generates* a signal with artificial periodicity and large amplitude oscillations (much higher spectral components in Fig. 7, left panel). The right panel of Fig. 7 shows the superposition of the spectra obtained with the acceptable time steps: $t_s = 10^{-12}s$ (dashed line, red online), $t_s = 10^{-}14s$ (dotted line, green online) and $t_s = 10^{-16}s$ (solid line, blue online). Interestingly, the largest of these time steps ($t_s = 10^{-12}s$), deemed to be acceptable with the criteria of Section 2, shows a "resonance" peak at approximately $6GHz$ with amplitude nearly double that of the signal computed with the smaller steps (compatible with each other). In the rest of the spectrum (not shown) all integrations of the SREs provide a gradually decreasing trace practically indistinguishable for the three traces. Notice that in order to render the spectra more readable, we have performed a smoothing on 7 consecutive points on these spectra (right panel).

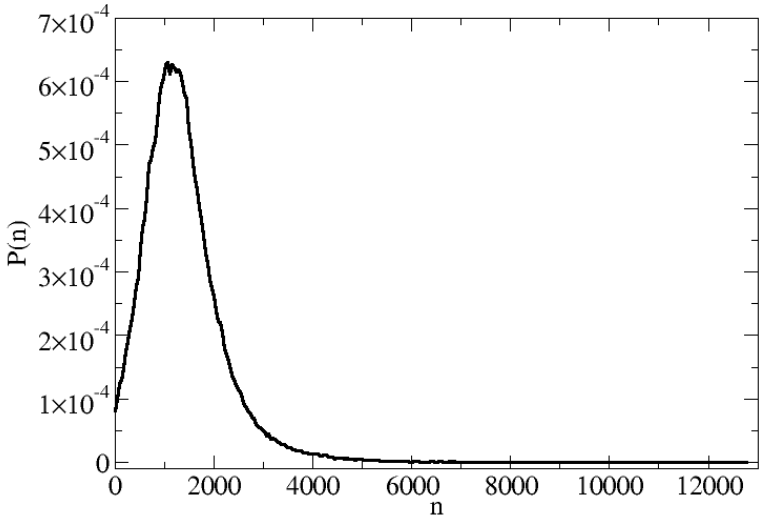


Figure 8. Histogram of the probability density of observing $n$ photons for an ensemble of 100 trajectories of duration $t_d = 100ns$ computed with time steps $t_s = 10^{-11}s$. The vertical axis is vertically shifted to highlight the long tail. The histogram is constructed on $N_b = 300$ bins. Parameters: $\gamma = 1 \times 10^9 s^{-1}$, $\Gamma_c = 10^{11}s^{-1}$, $R = 15 \times R_{th}$, $\beta = 10^{-2}$.

Finally, Fig. 8 shows the probability of observing $n$ photons under the same conditions as Fig. 2 but for a time step ($t_s = 10^{-11}$) which does not fulfill the conditions highlighted in Section 2. Notice the entirely different shape of the probability distribution which does not match those obtained with correct time steps (in the range $10^{-16}s \leq t_s \leq 10^{-12}s$) in spite of the fact that one could argue that the actual time scales of the laser (inverse photon relaxation rate $\Gamma_c^{-1} = 10^{-11}s$) is of the same order than the time step and one would expect the coupled time constant, $(\gamma\Gamma_c)^{-1/2}$, to be even better matched by this time step. This gives and additional proof of the criteria given in Section 2.

## 6. CONCLUSIONS

We have discussed in detail the implementation of the simplest possible stochastic numerical scheme for the integration of the laser rate equations. Issues related to the integration time step have been carefully discussed

and tested, finding that the general criterion (time step approximately ten times smaller than the fastest time constant) proven to satisfactorily reproduce the deterministic REs holds also in the SREs. We have further shown that failure to match this criterion amounts to artificially generating an inexistent deterministic dynamics with the stochastic integration. Minor changes in the spectral properties have been appeared for the largest integration step compatible with the previous criteria. A clear guide for the implementation of the correlated noise in the REs is given, accompanied by tests either of the simple (uncorrelated) stochastic scheme, as well as thorough checks on the convergence of both trajectories and statistical information gained from the SREs. The order of convergence for the Euler-Maruyama scheme is discussed together with a comparison of the order of the stochastic contribution, compared to the deterministic one.

GLL is very grateful to L. Gil for numerous discussions on the implementation of the numerical integration of stochastic equations.

## REFERENCES

[1] A.E. Siegman, *Lasers*, (University Science Books, Mill Valley, CA, 1986).
[2] L.M. Narducci and N.B. Abraham, *Laser Physics and Laser Instabilities*, (World Scientific, Singapore, 1988).
[3] J.R. Tredicce, F.T. Arecchi, G.L. Lippi, and G.P. Puccioni, "Instabilities in lasers with an injected signal", J. Opt. Soc. Am. **B2**, 173 (1985).
[4] D.E. McCumber, "Intensity fluctuations in the output of cw laser oscillators. I", Phys. Rev. **141**, 306 (1966).
[5] L.A. Coldren and S.W. Corzine, *Diode Lasers and Photonic Integrated Circuits*, (Wiley, New York, 1995).
[6] C.H. Henry, "Theory of the linewidth of semiconductor lasers", IEEE J. Quantum Electron. **18**, 259 (1982).
[7] P.R. Rice and H.J. Carmichael, "Photon statistics of a cavity-QED laser: A comment on the laser phase-transition analogy", Phys. Rev. A **50**, 4318 (1994).
[8] J. Mørk and G.L. Lippi, "Nanolaser rate equations and quantum noise properties", submitted to Applied Physics Letters.
[9] G.L. Lippi, J. Mørk, and G.P. Puccioni, in preparation.
[10] A. Rößler, "Runge–Kutta methods for Itô stochastic differential equations with scalar noise", BIT Numerical Mathematics **46**, 97 (2006).
[11] X. Wang and S. Gan, "A Runge–Kutta type scheme for nonlinear stochastic partial differential equations with multiplicative trace class noise", Numer. Algor. **62**, 193 (2013) and references therein (particularly the review [7]).
[12] O. Svelto, *Principles of Lasers*, 5$^{\text{th}}$ ed. (Springer, Berlin, 2010).
[13] N.J. van Druten, Y. Lien, C. Serrat, S.S.R. Oemwrawsingh, M.P. van Exter, and J.P. Woerman, "Laser with thresholdless intensity fluctuations", Phys. Rev. A **62**, 053808 (2000).
[14] G.L. Oppo and A. Politi, "Improved adiabatic elimination in laser equations", Europhys. Lett. **1**, 549 (1986).
[15] H.G. Solari, M.A. Natiello, and G.B. Mindlin, *Nonlinear dynamics: a two-way trip from physics to math*, (Taylor & Francis, New York, 1996).
[16] A. Einstein, "Über die von der molekularkinetischen Theorie der Wärme geförderte Bewegung von in ruhenden Flüssigkeiten suspendierten Teilchen", Ann. Physik **322**, 549 (1905).
[17] K. Huang, *Introduction to Statistical Physics*, (Taylor & Francis, New York, 2001).
[18] https://en.wikipedia.org/wiki/Euler%E2%80%93Maruyama_method – consulted on February 4, 2018.
[19] J. Palczewski, Lecture 5: *Numerical schemes for SDEs* – https://www.mimuw.edu.pl/ãpalczew/CFP_lecture5.pdf; consulted on February 11, 2018.
[20] M. Matsumoto and T. Nishimura, "Mersenne Twister: A 623-dimensionally equidistributed uniform pseudorandom number generator, ACM Transactions on Modeling and Computer Simulation **8** (1), 3–30 (1998).